CANCER BIOTHERAPY AND RADIOPHARMACEUTICALS
Volume 24, Number 5, 2009

DOI: 10.1089/cbr.2008.0606

Research Article

A ^{99m}Tc-Labeled Triphenylphosphonium Derivative for the Early Detection of Breast Tumors

Zhixin Li,[1,*] Marcos Lopez,[1,2,*] Micaël Hardy,[1,2,*] Donna M. McAllister,[1] Balaraman Kalyanaraman,[1,2] and Ming Zhao[1,*]

Abstract

Introduction: A greater mitochondrial membrane potential in tumor cells has been shown to enhance the accumulation of triphenyl phosphonium derivatives. The aim of this study was to synthesize and characterize ^{99m}Tc-labeled alkyl triphenyl phosphonium (^{99m}Tc-Mito$_{10}$-MAG3) for the early detection of breast tumors.
Methods: Mito$_{10}$-MAG3 was synthesized by coupling (10-aminodecyl)triphenyl phosphonium bromide with NHS-MAG3 and radiolabeled with ^{99m}Tc. Biodistribution and pharmacokinetics of ^{99m}Tc-Mito$_{10}$-MAG3 was investigated in female Sprague-Dawley rats. Initially, ^{99m}Tc-Mito$_{10}$-MAG3 was tested in animals with established breast tumors. In a subsequent longitudinal study, the imaging efficacy of ^{99m}Tc$_{10}$-Mito-MAG3 for detecting small, nonpalpable breast tumors was assessed after chemically inducting breast carcinoma. Tumors detected by imaging were allowed to grow to palpable size and confirmed by histology. The results were compared with ^{99m}Tc-MIBI.
Results: The synthesis of Mito$_{10}$-MAG3 was confirmed by mass spectrometry. The compound was radiolabeled with ^{99m}Tc to $>92\%$ in a single step. The radiopharmaceutical exhibited fast blood clearance and low cardiac uptake. In the initial study, using animals with established breast tumors, ^{99m}Tc-Mito$_{10}$-MAG3 imaging detected small lesions that were missed by palpation. In the longitudinal study, ^{99m}Tc-Mito$_{10}$-MAG3 exhibited focal uptake in small breast tumors, which were confirmed by histology.
Conclusions: Imaging, using ^{99m}Tc-Mito$_{10}$-MAG3, allowed the early detection of small neoplastic lesions in the mammary glands. The agent significantly reduced cardiac uptake, compared with ^{99m}Tc-MBIB. The phosphonium-based derivatives warrant further characterization and development as imaging agents for scintimammography.

Key words: scintimammography, breast cancer, DMBA, mitochondria

Introduction

Breast cancer is among the most commonly diagnosed cancers and has the second highest mortality rate in females in the United States.[1,2] Early, accurate diagnosis of breast cancer is critical to successful intervention. Scintimammography is an adjunct diagnostic tool for patients with suspected breast cancers.[3–5] The technique provides physiologic information about the target tissue by utilizing mitochondria-targeting tracers.[5–7]

Currently, the main imaging agents in scintimammography are ^{99m}Tc-methoxyisobutylisonitrile (^{99m}Tc-MIBI) and ^{99m}Tc-tetrofosmin.[8,9] Originally developed as heart-imaging agents, the elevated uptake of these mitochondria-targeting agents in carcinomas is positively correlated to cancer invasiveness and is attributed to active angiogenesis and an aberrant oxidative metabolism of tumor cells.[10,11] For breast imaging, however, the cardiac and hepatic uptake of the existing agents is relatively high, which tends to cause background issues due to the close proximity to mammary

[1]Department of Biophysics, Medical College of Wisconsin, Milwaukee, Wisconsin.
[2]Free Radical Research Center, Medical College of Wisconsin, Milwaukee, Wisconsin.
*Co-first authorship.

Address Correspondence to: Ming Zhao; Department of Biophysics, Medical College of Wisconsin, 8701 Watertown Plank Road, Milwaukee, WI, 53226
E-mail: **mzhao@mcw.edu**

tissues. There remains a technical drive to explore newer agents that may lead to improved imaging quality.

This study aimed to investigate the potential of a ^{99m}Tc-labeled triphenyl phosphonium (TPP) cation-based mitochondria imaging agent for the early detection of breast tumors. ^{99m}Tc is widely available with established radiochemistry. In addition, the rationale of testing TPP derivatives stems from reports that the membrane potential from outside the cell to mitochondria in tumor cells is at least 60 mV greater (i.e., more negative) than in the mitochondria from normal cells.[12,13] Consequently, because of their membrane potential-dependent uptake activity, TPP derivatives accumulate approximately 10-fold higher in tumor-cell mitochondria.[13–16] As established mitochondria-targeting vectors, the TPP compounds are attractive alternatives to the existing imaging agents. In this article, we describe the synthesis and characterization of a ^{99m}Tc-labeled TPP derivative, Mito$_{10}$-MAG3. The compound consists of a triphenyl phosphonium head group as the targeting vector, a 10-carbon alkly linker, and a MAG3 as the chelation site for ^{99m}Tc. The use of ^{99m}Tc-Mito$_{10}$-MAG3 enabled the detection of small breast tumors on the milligram level in a rat model of chemically induced breast carcinomas. In addition, ^{99m}Tc-Mito$_{10}$-MAG3 has significantly reduced cardiac uptake, compared with ^{99m}Tc-MIBI. These results demonstrated potential in overcoming some of the challenges for existing scintimammography-imaging agents.

Methods

Synthesis of Mito$_{10}$-MAG3

All reagents were used as received without further purification. The reactions were monitored by thin-layer chromatography on silica gel and by high-performance liquid chromatography (HPLC). Crude materials were purified by flash chromatography on silica gel 60 (0.040–0.063 mm). Characterization was performed on HPLC) and high-resolution mass spectrometry (HRMS) for all products. HPLC experiments were performed by using an Agilent 1100 system equipped with UV-Vis absorption and fluorescence detectors, using a C_{18} column (Kromasil, 250×4.6 mm, 5 μm; Alltech, Deerfield, IL) that was equilibrated with 10% CH_3CN [containing 0.1% (v/v) trifluoroacetic acid (TFA)] in 0.1% TFA aqueous solution. Approximately 40 minutes after injection, the CH_3CN fraction was increased to 100% and the

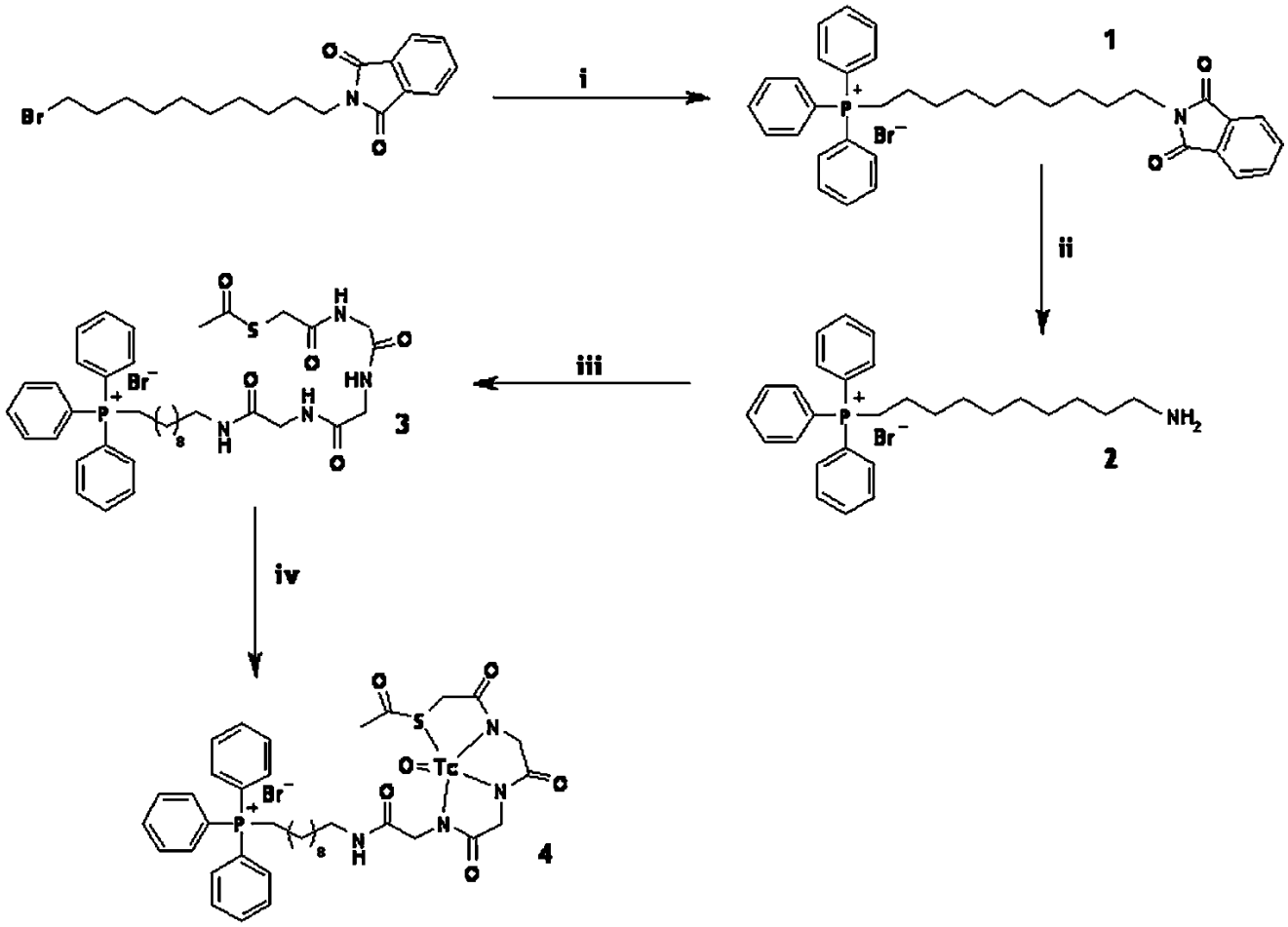

FIG. 1. Schematic drawing of the chemical synthesis and radiolabeling of Mito$_{10}$-MAG3. (10-phtalimidyl) triphenyl phosphonium bromide [**1**] was synthesized in reaction (1) from (10-bromodecyl)phthalimide and triphenyl phosphine. (10-aminodecyl) triphenyl phosphonium bromide [**2**] was synthesized in reaction (2) by using hydrazine. Mito$_{10}$-MAG3 was produced by reaction (3) involving NHS-MAG3 and (10-aminodecyl) triphenyl phosphonium bromide [**3**]. The ^{99m}Tc-chelated form of Mito$_{10}$-MAG3 is shown as [**4**].

compounds were eluted by using a flow rate of 0.5 mL/min. Mass spectra were obtained by using the 7.0 Tesla Fourier Transform Ion Cyclotron Resonance (FT-ICR) Mass Spectrometer (Applied Biosystems, Foster City, CA) interfaced with an Agilent 1100 HPLC system. (Santa Clara, CA).

$Mito_{10}$-MAG3 was synthesized according to the protocol depicted in Figure 1. N-hydroxysuccinamide ester activated mercaptoacetyltriglycine (NHS-MAG3) was synthesized, as previously described, with minor modifications.[17]

(10-phtalimidyl) triphenylphosphonium bromide (1). A mixture containing bromodecyl phtalimide (7 g, 0.019 mol) and triphenylphosphine (5 g, 0.019 mol) in acetonitrile (60 mL) was refluxed for 15 hours. The solvent was distilled under reduced pressure. The crude product was purified by flash chromatography on silica gel (CH_2Cl_2/EtOH; 80:20) afforded a white solid 1 (9 g, 73%). MS calculated for $[C_{36}H_{39}NO_2P]^+$, Br^-; $[C_{36}H_{39}NO_2P]^+$, 548.3; found: 548.3.

(10-aminodecyl) triphenylphosphonium bromide (2). To a solution of **1** (7 g, 0.0108 mol) in EtOH (70 mL) was added hydrazine (0.54 mL, 0.0108 mol). The mixture was refluxed for 15 hours. The solvent was distilled and the impurity was crystallized, using a mixture Et_2O/EtOH (100 mL + 45 mL). The product was purified by flash chromatography on silica gel (CH_2Cl_2/EtOH; 80:20) afforded a yellow solid **2** (4 g, 73%). ^{31}P-NMR (nuclear magnetic resonance) (121.49 MHz) δ 24.61. ^{1}H-NMR (300.13 MHz) δ 7.95–7.73 (15H, m), 3.70–3.55 (2H, m), 2.80–2.70 (2H, m), 1.60–1.40 (6H, m), 1.35–1.10 (10H, m). MS calculated for $[C_{28}H_{37}NP]^+$, Br^-; $[C_{28}H_{37}NP]^+$, 418.2; found: 418.2.

Mito-MAG_3 (3). To a mixture of NHS-MAG3 (0.100 g, 0.25 mmol) and (10-aminodecyl) triphenylphosphonium bromide **2** (0.123 g, 0.25 mmol) in dimethyl sulfoxide (DMSO) (10 mL) was added at room temperature under inert-atmosphere triethylamine (82 μL, 0.60 mmol). The reaction mixture was stirred for 12 hour, and then the solvent was distilled under a high vacuum. Purification of the crude product by preparative HPLC, using a C_{18} column, afforded a white powder (0.097 g, 50%), corresponding to Mito-MAG_3 **3**. HRMS calculated for $C_{38}H_{50}N_4O_5PS$, $[C_{38}H_{50}N_4O_5PS]^+$: 705.3229; found: 705.1130. HPLC, 33.58 minutes.

Radiolabeling of $Mito_{10}$-MAG3

$Mito_{10}$-MAG3 was radiolabeled with ^{99m}Tc, using a protocol previously reported, with minor modifications.[17] Specifically, an aliquot of $Mito_{10}$-MAG3 (30 μg) was resuspended in 450 μL of freshly prepared labeling solution containing 7.5 mg of tartaric acid, 9.5 mg of ammonium acetate, and 10 μg of stannous chloride (pH, 8.3). After the addition of ^{99m}Tc pertechnetate (3 mCi), the labeling mixture was incubated at 65°C for 1 hour. For quality-control purposes, the radiolabeled product was routinely analyzed by radio, HPLC (4.6×250 mm C18 reversed-phase column) at room temperature, with the following method. Buffer A consisted of 10 mM of phosphate buffer (pH 6.8), and buffer B was 100% acetonitrile. A baseline of 90% A and 10% B was run for 10 minutes, followed by a linear gradient with the mobile phase reaching 10% A and 90% B at 40 minutes. To determine the radiostability, the radiopharmaceutical was maintained in physiologic buffer for up to 48 hours, and the radiochemical purity was examined by radio-HPLC.

Biodistribution and pharmacokinetics in rats

^{99m}Tc-$Mito_{10}$-MAG3 was injected into healthy rats (female Sprague-Dawley, 250–300 g) via the tail vein. Rats ($n = 3$) were sacrificed at 1, 3, 5, 10, 30, and 60 minutes after injection, and the distribution of radioactivity in different tissues was determined by gamma-well counting, with an energy window of 140 ± 15 keV. The biodistribution data were expressed in terms of percent injected dose per gram (%ID/g), with mean plus standard deviation. Urine samples were collected from the bladder at 30 minutes after injection and were analyzed by radio-HPLC to determine the presence of metabolic derivatives of the radiotracer. Tracer kinetics and biodistribution profile were confirmed by using *in vivo* scintigraphic imaging. Specifically, anterior planar whole-body dynamic images were acquired on an XRT gamma camera (General Electric, Waukesha, WI), using a high-resolution, medium-energy, parallel-hole collimator at one frame per minute for 60 minutes, with 512×512 matrix, and an energy window of 140 ± 15 keV.

In vivo *studies using a chemically induced breast tumor model in rats*

The animal protocol was approved by the institutional animal care and use committee (IACUC) review and followed the National Institutes of Health (NIH) guidelines. The rat model of 7,12 dimethyl-benz[a]anthracene (DMBA)-induced breast carcinoma was used.

As an initial feasibility study, rats were induced with 65 mg/kg of DMBA dissolved in sesame oil via a single oral gavage to the stomach. Eleven (11) weeks later, 3 rats with established breast carcinoma (0.5–1.9 cm in diameter) were imaged after a ^{99m}Tc-$Mito_{10}$-MAG3 injection (10 μg, 1 mCi), using a constant-rate infusion pump for a total injection volume of 150 μl over a period of 35 minutes. Static images were acquired on a GE XRT gamma camera, using a high-resolution, parallel-hole collimator, with a 512×512 matrix size, 22.5×22.5 cm field of view, 140 ± 15 keV energy window, and 100 k counts. Unexpectedly, apart from the established palpable carcinomas, additional small (i.e., millimeter size) tumors were discovered by this imaging technique in the same animals. This finding promoted a longitudinal study to investigate the early detection of neoplastic growth by using ^{99m}Tc-$Mito_{10}$-MAG3.

Six (6) 48-day-old rats were injected with 65 mg/kg of DMBA. At each week after DMBA induction, the rats were imaged by using the following protocol. Each rat was anesthetized with 1.6% isoflurane in room air supplemented with oxygen. The rat was immobilized in a prone position on the surface of the gamma-camera. ^{99m}Tc-$Mito_{10}$-MAG3 (10 μg, 1 mCi) was injected via the tail vein, using a constant-rate infusion pump, for a total injection volume of 150 μL over a period of 35 minutes. The continuous-infusion method was used to partially compensate for a fast blood clearance of the agent and to enhance a sustained tumor uptake. Dynamic images were continuously acquired at one frame per minute for 90 minutes, using the imaging parameters described above. The weekly imaging regiment was continued for all 6 rats until palpable tumors became detectable, which

typically takes place between 7 and 9 weeks after the administration of DMBA. Due to the relatively short physical half-life of ^{99m}Tc (6 hours), no residual signal, and therefore, no cross-contamination, is detectable from the previous injection the week before.

Comparison with ^{99m}Tc-MIBI

^{99m}Tc-MIBI of clinical formulation was purchased from Bristol-Myers Squibb (New York). At 48 hours after the breast tumors were first identified by using ^{99m}Tc-Mito$_{10}$-MAG3, the same rats were injected with ^{99m}Tc-MIBI (1 mCi per rat) via the tail vein. At this time, the radioactivity from the ^{99m}Tc-Mito$_{10}$-MAG3 injection already had cleared to background from the animals due to physical decay and excretion. Dynamic images were acquired in an identical fashion following ^{99m}Tc-MIBI injection.

Imaging data analysis

Since the typical biodistribution of a lipophilic radiopharmaceutical in the abdominal region precludes reliable imaging of breast tissues below the diaphragm, mammary glands that are located below the thorax were excluded from the data analysis.

Imaging data analysis was carried out by using an in-built software, by carefully drawing a region of interest (ROI) on the tumor site to determine the radioactivity counts in the ROI. ROIs with identical geometry and number of pixels were positioned on the contralateral normal mammary gland and the thigh muscle. Radioactivity counts were determined in each ROI. The tumor-to-normal and tumor-to-muscle ratios were calculated as the count ratio between the two ROIs.

Histology

The rats were sacrificed by CO_2 asphyxiation, and the number and location of the mammary tumors were recorded at necropsy. The tumors were dissected, with the diameter and weight measured and documented. Portions of each tumor were fixed in 10% formalin and embedded in paraffin. Histologic sections (at 5 μm thick) were prepared and stained with hematoxylin and eosin (H&E), according to standard histologic protocol. Pathologic diagnoses of the mammary lesions were classified by a certified pathologist.

Results

Synthesis and characterization of Mito$_{10}$-MAG3

The chemical yield and molecular weights (MWs) of the intermediates and final compound were as follows. **1.** yield, 73%; calculated MW for $[C_{36}H_{39}NO_2P]^+$, Br^-; $[C_{36}H_{39}NO_2P]^+$, 548.3; found: 548.3. **2.** yield, 73%; calculated MW for $[C_{28}H_{37}NP]^+$, Br^-; $[C_{28}H_{37}NP]^+$, 418.2; found: 418.2. **3.** yield, 50%; calculated MW for $C_{38}H_{50}N_4O_5PS$, $[C_{38}H_{50}N_4O_5PS]^+$: 705.3229; found: 705.1130. The structure of Mito$_{10}$-MAG3 was confirmed by ^{31}P- and ^{1}H-NMR with the following findings. ^{31}P-NMR (121.49 MHz) δ 24.27. ^{1}H-NMR (300.13 MHz) δ 9.05 (1H, t, $J = 5.3$), 8.31 (1H, t, $J = 5.8$), 8.18 (1H, t, $J = 6.6$), 7.90–7.62 (15H, m), 7.06 (1H, t, $J = 5.5$), 3.98 (2H, d, $J = 5.\ 8$), 3.82 (4H, 2d, $J = 6.\ 6, 5.3$), 3.67 (s, 2H), 3.40–3.28 (2H, m), 3.21 (2H, q, $J = 6.4$, 12.6), 2.35 (3H, s), 1.60–1.45 (6H, m), 1.35–1.20 (10H, m).

Radiolabeling

Mito$_{10}$-MAG3 was labeled with ^{99m}Tc to relatively high radiochemical purity and yield in a single step. According to radio-HPLC analysis, the radiochemical purity was consistently greater than 92%. At the current labeling condition, the specific activity was about 100 Ci/g. Once labeled, the radiopharmaceutical was stable in physiologic solution for an extended period of time without degradation. This was confirmed by using radio-HPLC, where the percentage of radioactivity bound to Mito$_{10}$-MAG3 remained persistent for at least 48 hours after labeling.

Table 1. Biodistribution of ^{99m}Tc-Mito$_{10}$-MAG3 in Rats in Terms of %ID/g

	Radioactivity uptake (%ID/g)					
Organ	*1 minute*	*3 minutes*	*5 minutes*	*10 minutes*	*30 minutes*	*60 minutes*
Brain	0.04 ± 0.03	0.02 ± 0.01	0.04 ± 0.03	0.01 ± 0.00	0.01 ± 0.01	0.00 ± 0.00
Thyroids	0.30 ± 0.13	0.33 ± 0.07	0.27 ± 0.11	0.11 ± 0.04	0.02 ± 0.02	0.01 ± 0.00
Lung	0.82 ± 1.05	0.31 ± 0.14	0.48 ± 0.43	0.23 ± 0.24	0.05 ± 0.01	0.03 ± 0.01
Heart	0.20 ± 0.08	0.27 ± 0.04	0.18 ± 0.07	0.06 ± 0.01	0.02 ± 0.02	0.01 ± 0.00
Liver	3.23 ± 1.10	2.41 ± 1.12	1.50 ± 0.84	0.89 ± 0.30	0.32 ± 0.02	0.21 ± 0.07
Pancreas	0.32 ± 0.22	0.27 ± 0.12	0.20 ± 0.17	0.12 ± 0.04	0.01 ± 0.00	0.02 ± 0.01
Spleen	0.27 ± 0.12	0.25 ± 0.17	0.20 ± 0.08	0.09 ± 0.04	0.02 ± 0.02	0.02 ± 0.01
Kidneys	2.30 ± 0.55	3.69 ± 0.92	3.06 ± 1.41	1.79 ± 0.39	1.40 ± 0.96	0.75 ± 0.59
Stomach	0.26 ± 0.04	0.32 ± 0.12	0.25 ± 0.26	0.30 ± 0.24	0.57 ± 0.41	0.04 ± 0.05
Small intestine	0.18 ± 0.04	0.67 ± 0.30	0.48 ± 0.14	0.50 ± 0.19	0.52 ± 0.20	0.36 ± 0.41
Colon	0.09 ± 0.04	0.08 ± 0.03	0.02 ± 0.01	0.03 ± 0.01	0.04 ± 0.03	0.01 ± 0.00
Bone	0.12 ± 0.05	0.05 ± 0.01	0.02 ± 0.24	0.04 ± 0.03	0.01 ± 0.01	0.00 ± 0.00
Muscle	0.05 ± 0.02	0.03 ± 0.01	0.06 ± 0.01	0.06 ± 0.01	0.02 ± 0.01	0.01 ± 0.00
Fat	0.04 ± 0.02	0.06 ± 0.01	0.07 ± 0.05	0.07 ± 0.03	0.01 ± 0.00	0.00 ± 0.00
Skin	0.07 ± 0.03	0.10 ± 0.04	0.12 ± 0.08	0.05 ± 0.04	0.04 ± 0.03	0.02 ± 0.01
Thymus	006 ± 0.02	0.12 ± 0.04	0.07 ± 0.01	0.04 ± 0.03	0.01 ± 0.00	0.01 ± 0.00
Urine	0.05 ± 0.05	0.76 ± 0.56	0.68 ± 0.03	2.35 ± 2.63	8.83 ± 8.50	10.85 ± 12.48

Each data point represents the mean uptake with standard deviation from 3 animals.

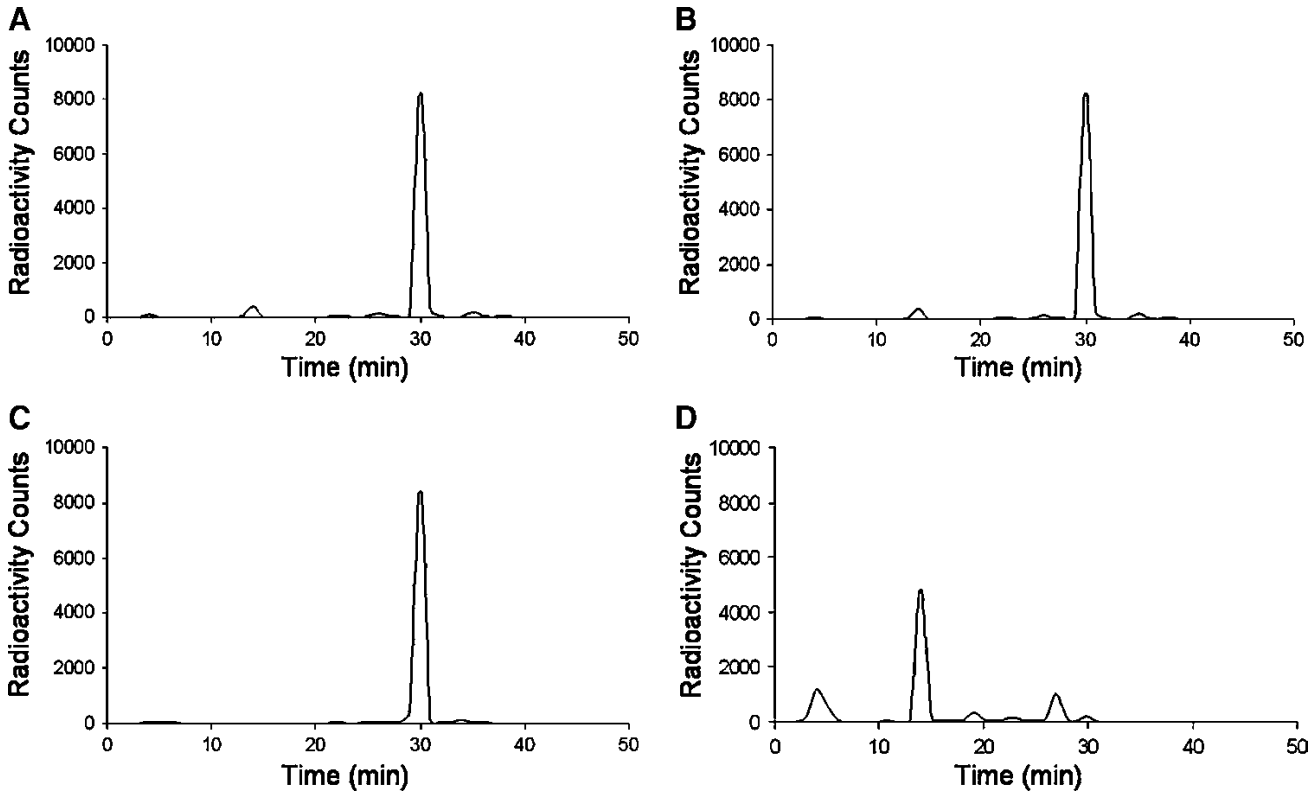

FIG. 2. Radiochemical stability and pharmacokinetics of ^{99m}Tc-Mito$_{10}$-MAG3. (A–C) radio-HPLC chromatogram of ^{99m}Tc-Mito$_{10}$-MAG3 at 0, 24, and 48 hours (A–C) after radiolabeling, where there was no significant change in radiochemical purity. (**D**) radio-HPLC chromatogram of a urine sample taken at 30 minutes after the intravenous injection of ^{99m}Tc-Mito$_{10}$-MAG3, where the radioactive metabolites are present. HPLC, high-performance liquid chromatography.

Biodistribution and pharmacokinetics

The intravenous injection of ^{99m}Tc-Mito$_{10}$-MAG3 was followed with a prompt blood clearance, where the blood half-life was estimated to be less than 2 minutes. It is notable that the myocardial uptake of the tracer was relatively low, peaking at 0.27 ± 0.04 %ID/g at 3 minutes after injection (Table 1). A continuous washout reduced the myocardial radioactivity level to 0.06 ± 0.01 and 0.02 ± 0.02 %ID/g at 10 and 30 minutes after injection. Other tissues in the thoracic region, including the lungs, muscle, thymus, thyroid, and bones, were low in radioactivity uptake. The bulk of the injected dosage was initially collected in the liver and the kidneys, where hepatic and renal clearance were the main routes of clearance (Table 1). Once taken up in the liver, the radioactivity rapidly transitioned to the gastrointestinal tract, accompanied with a fast decline of hepatic signal from 3.23 ± 1.10 %ID/g at 1 minutes to 0.32 ± 0.02 %ID/g at 30 minutes after injection. The biodistribution profile was confirmed by whole-body dynamic imaging, where the radiotracer rapidly cleared from the hepatic/gastrointestinal and renal/urinary systems, leaving a low general background in the thorax region. The metabolized radioactive species of the radiopharmaceutical were detected in urine samples by radio-HPLC (Figure 2).

In a comparative study, the myocardial uptake of ^{99m}Tc-MIBI peaked at 2.70 ± 0.4 %ID/g within minutes after injection and remained above 2.41 ± 0.3 %ID/g for at least 90 minutes. Comparatively, the myocardial uptake level of ^{99m}Tc-Mito$_{10}$-MAG 3 was 10-, 40-, and 120-fold lower than that of ^{99m}Tc-MIBI at 3, 10, and 30 minutes after injection. The hepatic uptake of ^{99m}Tc-MIBI was at 0.37 ± 0.14 %ID/g at 30 minutes after injection.

In vivo *imaging of chemically induced tumors in a rat breast cancer model*

As a feasibility study, 3 rats with established breast carcinomas (average size, 0.5–1.9 cm in diameter) were imaged with ^{99m}Tc-Mito$_{10}$-MAG3 at 11 weeks after DMBA induction. Unexpectedly, apart from the known tumor sites at mammary glands Rc and Rf, two well-defined focal uptake areas of the radiotracer were detected in the same animals at mammary glands La and Re (Fig. 3). Histologic analysis confirmed the presence of papillary carcinoma at La, Rc, and Rf, while the mammary tissue from the contralateral side (gland Le) was used as the control (Fig. 3E). The size of the small tumor at La at the time of dissection was $2.5 \times 5.9 \times 1.9$ mm, weighing 18 mg. A focal radioactivity uptake at Re, but histologically equivocal, was marked with a block arrow. In light of these findings, a longitudinal study that focused on detecting breast carcinoma at an early growth phase was carried out.

In the longitudinal study, of the 6 rats enrolled, four sites of neoplastic growth were induced in mammary glands a and b. Using ^{99m}Tc-Mito$_{10}$-MAG3, all 4 tumors were detected

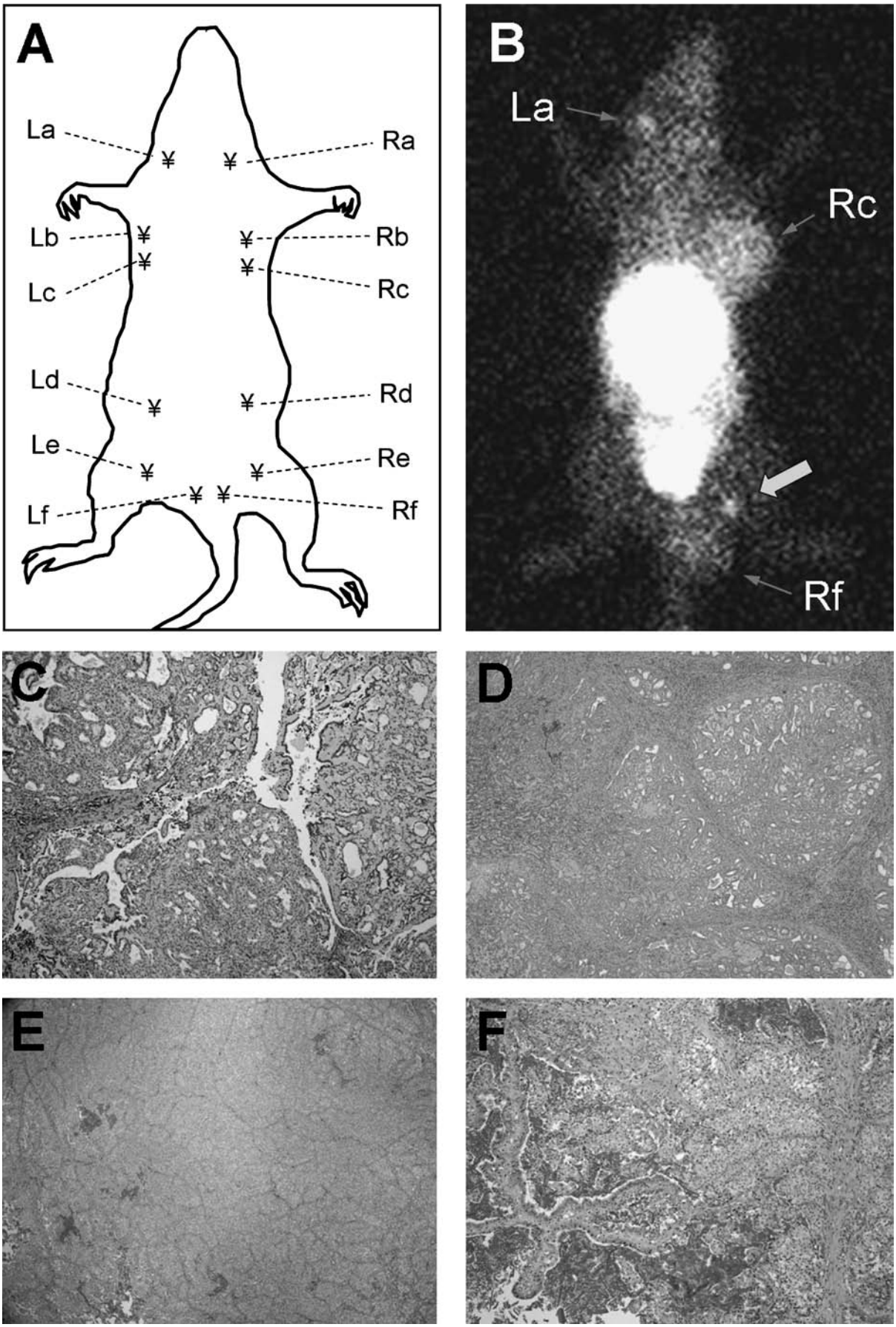
A
La
Ra
Lb
Rb
Lc
Rc
Ld
Rd
Le
Re
Lf
Rf
B
La
Rc
Rf
C
D
E
F

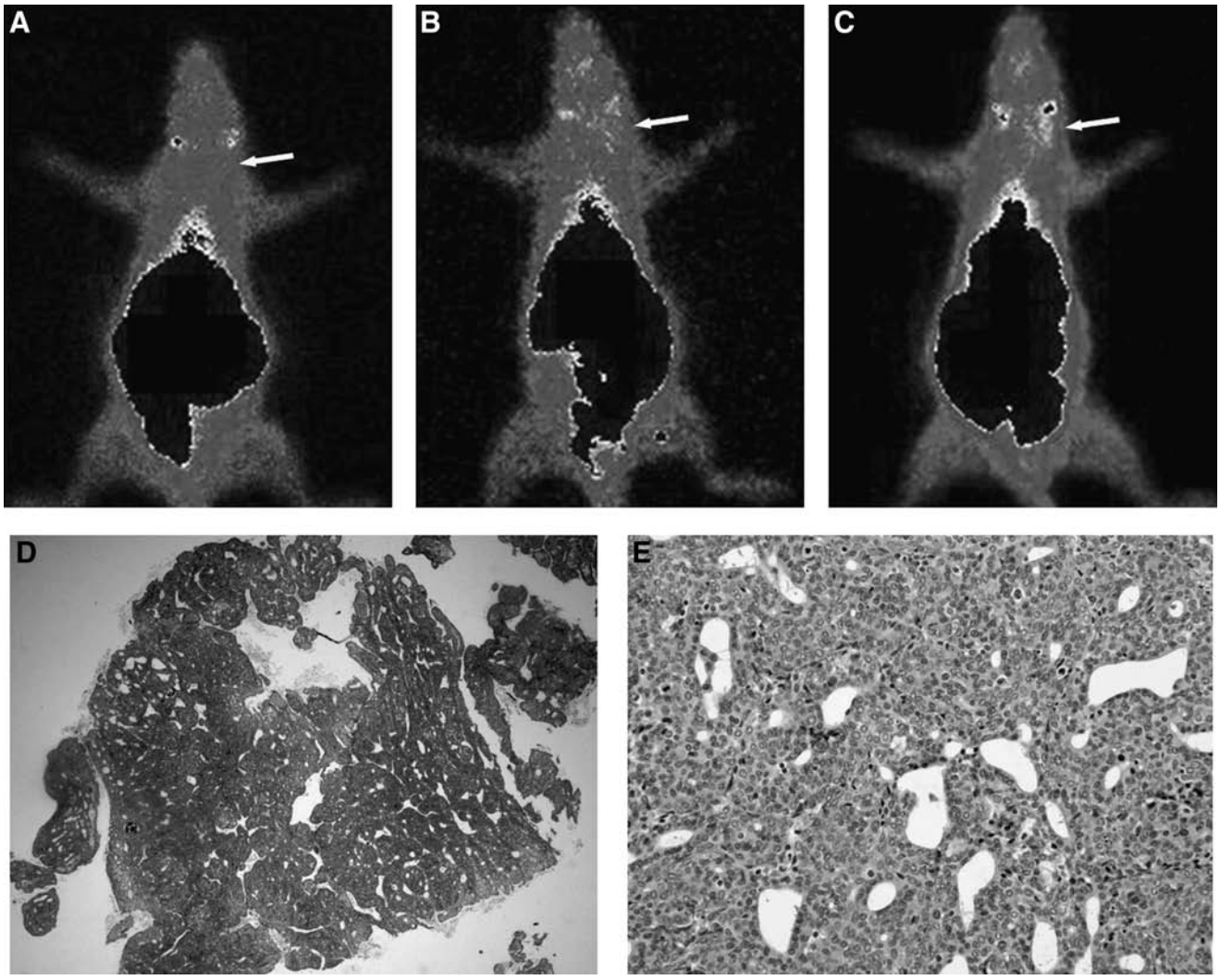

FIG. 4. An example of the longitudinal study, using ^{99m}Tc-Mito$_{10}$-MAG3 for the early detection of early breast carcinomas in a DMBA-induced rat breast cancer model. Anterior images of the same rat from 3 consecutive weeks are shown in (**A–C**). The site of progressive tumor growth, as detected by ^{99m}Tc-Mito$_{10}$-MAG3, is marked by an arrow. hematoxylin and eosin–stained gross tumor morphology and cellular carcinogenesis of papillary carcinoma are shown in (**D**) and (**E**), respectively.

as focal radioactivity uptake at least 1 week earlier than by palpation. The tumor-to-normal and tumor-to-muscle ratios were 2.39 ± 0.77 and 6.61 ± 1.74, respectively, at the time of detection. This ratio was similar to that obtained by ^{99m}Tc-MIBI injection (2.04 ± 0.49 and 5.10 ± 0.31). The suspicious sites were allowed to develop until the carcinomas became detectable by palpation. Postmortem histologic analysis confirmed the presence of breast tumors. Of the 4 sites, 3 were papillary carcinoma, and 1 was atypical *in situ* ductal hyperplasia. A typical example of *in vivo* imaging, and the corresponding histology, is demonstrated in Figure 4. Consecutive weekly imaging results are shown in Figure 4A–4C, where elevating radioactivity uptake at the site of tumor development is marked by an arrow. The presence of papillary carcinoma at the right mammary gland "a" was confirmed by H&E stained histology, which demonstrates the gross tumor morphology and, at a higher magnification, cellular carcinogenesis in Figure 4D and 4E, respectively.

Discussion

The current study was focused on investigating the potential of ^{99m}Tc-labeled TPP cation-based mitochondria agents for early breast tumor detection. Initial studies of

FIG. 3. Noninvasive detection of established palpable and nonpalpable early-growth breast carcinomas in DMBA-induced rat breast cancer model. (**A**) An illustration of the distribution of mammary glands on a female rat. (**B**) Anterior planar image of a tumor-bearing rat acquired after the intravenous injection of ^{99m}Tc-Mito$_{10}$-MAG3. A suspected, but equivocal, site is marked by a block arrow. (**C**) An early-growth breast carcinoma at mammary gland La is confirmed by histology, correlating to a focal radioactivity uptake in the planar image. (**D**) Histology of an established breast tumor at gland Rc. (**E**) Histology of normal mammary tissue harvested from gland Le. (**F**) Histology of an established breast carcinoma at gland Rf.

^{99m}Tc-Mito$_{10}$-MAG3 revealed some intriguing properties of this radiopharmaceutical, as follows. 1) While the tumor-to-nontumor ratio was similar for ^{99m}Tc-Mito$_{10}$-MAG3 and ^{99m}Tc-MIBI, the former had a cardiac uptake that was 1–2 orders of magnitude lower. This property would likely result in an improved detection sensitivity in the inferior portions of human mammary tissues, where a high cardiac uptake would otherwise cause background issues due to its close proximity; 2) ^{99m}Tc-Mito$_{10}$-MAG3 exhibited a fast blood clearance, with a blood half-life of less than 2 min in rats; and 3) The tumor uptake of ^{99m}Tc-Mito$_{10}$-MAG3 was followed by a washout, which suggests that an active transport mechanism may have been in place to remove the agent from intracellular compartments. A similar observation has been documented for other cationic lipophilic agents, where they are recognized as substrates for P-glycoprotein-dependent efflux.[18]

It is notable that the DMBA-induced breast carcinoma in rats in the *in vivo* longitudinal study is a relevant disease model in assessing the diagnostic efficacy of agents for scintimammography. In this model, the target of action by DMBA is the epithelial cells in the mammary gland.[19] As in human breast carcinoma, morphologically defined mammary lesions in DMBA-treated rats are initiated from the terminal-end buds or terminal ductules.[19,20] In this respect, the histogenic characteristics of DMBA-induced lesions in rats simulates that in the human counterpart, providing a realistic testing ground.

Apart from ^{99m}Tc-Mito$_{10}$-MAG3, it is conceivable that the imaging properties of TPP cation-based derivatives can be modulated by alternative chemical structures. The 10-carbon alkyl chain was selected for its mitochondria-targeting efficiency with minimial membrane toxicity.[21] This may be fine-tuned in terms of the number and types of functional groups between the TPP head group and the chelation site of the radioisotope.[21] It will be of interest to study and compare TPP derivatives of different sizes, hydrophobicity, electrostatic potentials, and chelation configurations. By screening a series of TPP agents, it is anticipated that a combination of synthetic chemistry and radiochemistry will lead to optimized imaging agents for early breast tumor detection.

Positron emission tomography (PET) constitutes an alternative radionuclide scintigraphic-imaging technique, using position-emitting radioisotopes. Recent studies reported TPP cation-derived radiopharmaceuticals labeled with ^{64}Cu for tumor imaging with excellent tumor-to-non tumor ratios.[22,23] Interestingly, ^{64}Cu-labeled TPP compounds exhibited comparable levels of myocardial uptake to ^{99m}Tc-Mito$_{10}$-MAG3. However, the tumor uptake of the PET-imaging agents experienced a delayed accumulation in the tumor, where the maximum radioactivity uptake was reached at a few hours after injection.[22] The difference in the tumor-uptake profiles between the two types of imaging agents may be explained by the following possibilities. First, differences in tumor types (U87MG human glioma xenografts in mice versus DMBA-induced breast carcinomas in rats) may lead to variable uptake kinetics. Second, while the prior study used fully developed xenograft tumors, with an average weight of 300–600 mg, the current study focused on detecting breast carcinomas in an early growth phase.

Conclusions

In conclusion, we report the synthesis and initial characterization of a ^{99m}Tc-labeled TPP cation-based mitochondria-targeting agent, ^{99m}Tc-Mito$_{10}$-MAG3, as a potential candidate for breast tumor detection. The agent has substantially lower cardiac uptakecompared with ^{99m}Tc-MIBI, while maintaining a tumor-avid binding activity in a DMBA-induced rat model of breast carcinoma. It is particularly noteworthy that imaging with ^{99m}Tc-Mito$_{10}$-MAG3 allowed the detection of early breast tumors in a relevant animal model. These findings indicate that the TPP cation-based radiopharmaceuticals hold potential as agents for breast tumor imaging and warrant further investigation.

Acknowledgments

Funding support from the National Institutes of Health (5RO1 CA077822-08) and the Medical College of Wisconsin Cancer Center is gratefully acknowledged. The authors thank the editorial assistance of Ms. Carrie O'Connor.

Disclosure Statement

No completing financial interests exist.

References

1. Parker S, Tong T, Bolden S, et al. Cancer statistics. CA Cancer J Clin 1997; 47:5.
2. Jemal A, Tiwari RC, Murray T, et al. Cancer statistics. CA Cancer J Clin 2004; 54:8.
3. Yang MD, Sun SS, Kao CH, et al. Usefulness of technetium-99m tetrofosmin scintimammography to detect breast cancer in mammographically dense breasts. Cancer Invest 2002; 20:518.
4. Khalkhali I, Baum JK, Villanueva-Meyer J, et al. ^{99m}Tc-sestamibi breast imaging for the examination of patients with dense and fatty breasts: Multicenter study. Radiology 2002; 222:149.
5. Khalkhali I, Cutrone JA, Mena I. Scintimammography: The complementary role of Tc-99m-sestamibi prone breast imaging for the diagnosis of breast carcinoma. Radiology 1995; 196:421.
6. Hussain R, Buscombe JR. A meta-analysis of scintimammography: An evidence-based approach to its clinical utility. Nucl Med Comm 2006; 27:589.
7. Mathieu I, Mazy S, Willemart B, et al. Inconclusive triple diagnosis in breast cancer imaging: Is there a place for scintimmography? J Nucl Med 2005; 46:1574.
8. Schillaci O, Buscombe JR. Breast scintigraphy today: Indications and limitations. Eur J Nucl Med Mol Imaging 2004; 31:S35.
9. Carvalho PA, Chiu ML, Kronauge JF, et al. Subcellular distribution and analysis of Tc-99m-MIBI in isolated perfused rat hearts. J Nucl Med 1992; 33:1516.
10. Delmon-Mongeon LI, Piwinica-Worms D, Van der Abbeele AD, et al. Uptake of the cation hexakis (2-methoxyisobutylisonitrile)-technetium-99m by human carcinoma cell lines *in vitro*. Cancer Res 1990; 50:2198.
11. Scopinaro F, Schillaci O, Scarpini M, et al. Technetium-99m-sestamibi: An indicator of breast cancer invasiveness. Eur J Nucl Med 1994; 21:984.
12. Kroemer G. Mitochondria in cancer. Oncogene 2006; 25: 4630.
13. Ross MF, Kelso GF, Blaikie FH, et al. Lipophilic triphenylphosphonium cations as tools in mitochondrial bioenergetics and free radical biology. Biochemistry 2005; 70:222.
14. Manetta A, Gamboa G, Nasseri A, et al. Novel phosphonium salts display *in vitro* and *in vivo* cytotoxic activity

against human ovarian cancer cell lines. Gynecol Oncol 1996; 60:203.
15. Smith RAJ, Kelso GF, James AM, et al. Targeting coenzyme Q derivatives to mitochondria. Meth Enzymol 2004; 382:45.
16. Sheu SS, Nauduri D, Anders MW. Targeting antioxidants to mitochondria: A new therapeutic direction. Bioc Bioph Acta 2006; 1762:256.
17. Wang Y, Liu X, Hnatowich DJ. An improved synthesis of NHS-MAG3 for conjugation and radiolabeling of biomolecules with (99m)Tc at room temperature. Nat Protoc 2007; 2:972.
18. Pwnica-Worms D, Chiu ML, Budding M, et al. Functional imaging of multidrug-resistant P-glycoprotein with an organotechnetium complex. Cancer Res 1993; 53:977.
19. Thompson HJ, Singh M. Rat models of premalignant breast disease. J Mammary Gland Biol Neoplasia 2000; 5:409.
20. Jordan VC. Laboratory models of breast cancer to aid the elucidation of antiestrogen action. J Lab Clin Med 1987; 109:267.
21. Nandi S, Guzman R C, Yang J. Hormones and mammary carcinogenesis in mice, rats, and humans: A unifying hypothesis. Proc Natl Acad Sci U S A 1995; 92:3650.
22. Wang J, Yang CT, Kim YS, et al. ^{64}Cu-labeled triphenylphosphonium and triphenylarsonium cations as highly tumor-selective imaging agents. J Med Chem 2007; 50:5057.
23. Kim YS, Yang CT, Wang J, et al. Effects of targeting moiety, linker, bifunctional chelator, and molecular charge on biological properties of (64)cu-labeled triphenylphosphonium cations. J Med Chem 2008; 51:2971.